



# Telmisartan-Loaded Lactosylated Chitosan Nanoparticles as a Liver Specific Delivery System: Synthesis, Optimization and Targeting Efficiency

Mohamed Nasr<sup>1,2</sup> · Ahmed Y. Kira<sup>2</sup> · Sameh Saber<sup>3</sup> · Ebtessam A. Essa<sup>4</sup> · Sanaa A. El-Gizawy<sup>4</sup>

Received: 26 April 2023 / Accepted: 8 June 2023 / Published online: 23 June 2023  
© The Author(s) 2023

## Abstract

Hepatocellular carcinoma (HCC) has a significant economic impact and a high mortality rate. Telmisartan (TLM) is a potential therapy for HCC, but it has a limited scope in drug delivery due to unpredictable distribution and poor bioavailability. The objective of this study was to prepare, design, and *in vitro* evaluate lactose-modified chitosan nanoparticles (LCH NPs) as a liver-targeted nanocarrier for TLM with the potential to offer a promising HCC therapy. The combination of chitosan with lactose was successfully attained using the Maillard reaction. TLM-LCH NPs were prepared, characterized, and optimized with the developed 2<sup>3</sup> full factorial design. The optimized formulation (F1) was *in vitro* and *in vivo* characterized. LCH was synthesized with an acceptable yield of 43.8 ± 0.56%, a lactosylation degree of 14.34%, and a significantly higher aqueous solubility (6.28 ± 0.21 g/L) compared to native chitosan (0.25 ± 0.03 g/L). *In vitro* characterization demonstrated that, F1 had a particle size of 145.46 ± 0.7 nm, an entrapment efficiency of 90.21 ± 0.28%, and a surface charge of +27.13 ± 0.21 mV. *In vitro* TLM release from F1 was most consistent with the Higuchi model and demonstrated significantly higher release at pH 5.5. Moreover, a significantly higher ratio of liver to plasma concentration was observed with TLM-LCH NPs compared to plain TLM and unmodified TLM-NPs. The obtained results nominate TLM-LCH NPs as a promising carrier for enhancing liver targeting of TLM in treatment of HCC.

**Keywords** active targeting · chitosan · lactose · Maillard reaction · telmisartan

## Introduction

The mammalian liver is an essential organ that removes harmful substances from the body's bloodstream, including drugs, organic waste products, and other foreign particles. Moreover, it helps with the anabolism of steroid hormones

and cholesterol. As the largest, most strategically positioned, and most multifunctional internal organ, the liver is susceptible to infections, injuries, and disorders. About 2 million people die every year from liver disease, whereas cirrhosis and liver cancer accounting for about 3.5% of all fatalities worldwide [1]. In addition to the high mortality risk, patients with liver diseases have a substantial economic impact and poor quality of life indices [2].

Telmisartan (TLM) belongs to the class of angiotensin II receptor blockers. It is an antihypertensive drug with a track record of clinical efficacy and safety. Besides, it has been found to have potential applications in several liver diseases, including non-alcoholic fatty liver disease [3], non-alcoholic steatohepatitis [4], alcoholic liver disease [5], and more interestingly, hepatocellular carcinoma (HCC) as an apoptotic agent [6]. However, TLM is a BCS class II drug, which has a limited scope in drug delivery caused by its poor solubility, poor bioavailability, and unpredictable biodistribution [7].

Most drugs reach a high concentration in the liver after being administered. However, due to their poor

✉ Mohamed Nasr  
m2nasr@yahoo.com

<sup>1</sup> Department of Pharmaceutics and Industrial Pharmacy, Faculty of Pharmacy, Helwan University, Cairo 11790, Egypt

<sup>2</sup> Department of Pharmaceutics, Faculty of Pharmacy, Delta University for Science and Technology, Gamasa 35712, Egypt

<sup>3</sup> Department of Pharmacology, Faculty of Pharmacy, Delta University for Science and Technology, Gamasa 35712, Egypt

<sup>4</sup> Department of Pharmaceutical Technology, Faculty of Pharmacy, Tanta University, Tanta 31111, Egypt

sensitivity and efficacy at usual doses, drugs used to treat liver diseases have often met with minimal success and a significant relapse rate. Furthermore, higher doses are frequently hampered by off-target safety issues, patient tolerability, and high resistance caused by efflux pumps (P-glycoprotein) [8]. Therefore, in order to address the highest therapeutic potential, many hepatic disorders require a high level of selectivity and accumulation within the relevant intrahepatic cells. These issues necessitate an effective drug delivery system that targets the liver.

In the last two decades, nanotechnology has led to an upsurge in drug delivery systems that specifically target the liver, these systems rely on altered biodistribution for enhanced hepatic therapeutic efficacy [9]. These systems can enhance liver drug accumulation owing to the physiological properties of the liver [10] and the physicochemical characteristics of the nanoparticles (NPs), which have a significant potential for more targeted-drug delivery: either passively or actively by conjugating tissue/cell-specific ligands to NPs. The most widely used approach for increasing the cellular uptake of NPs by hepatocytes is active targeting of the asialoglycoprotein receptors (ASGPR) [11]. ASGPR are primarily expressed by hepatocytes and is poorly distributed into extrahepatic tissues [12]. Indeed, each hepatocyte has approximately 500,000 ASGPR, which can detect and bind a wide spectrum of compounds exposing saccharide residues, including lactose [13, 14].

Since the physicochemical properties of polymeric NPs can be changed, including size, charge, and release behavior, they have been applied in various applications [15]. Most notably, the ease to be modified with different ligands for targeting specific receptors and have been extensively utilized for this purpose in liver targeting [16]. Recent years have seen a surge in interest in the use of chitosan NPs as a drug delivery vehicle due to their outstanding biodegradability and biocompatibility and the presence of reactive functional groups on their surfaces [17]. Chitosan NPs have been shown to have liver-targeting properties, and they were loaded with various actives for theranostic or therapeutic applications [18–21]. Recently, TLM loaded chitosan coated magnetic NPs were utilized as a colon-targeted drug delivery system [22].

This study focuses mainly on the decoration of chitosan with lactose molecules (LCH) as a liver-targeted nanocarrier for TLM that could enhance its localization inside liver tissues. In an effort to attain this objective, a 2<sup>3</sup> full factorial design was applied to fabricate and optimize TLM-LCH NPs. Furthermore, the optimized formulation was *in vitro* and *in vivo* characterized. It is expected that this will result in an improvement in the concentration of TLM within the liver, hence enhancing its potential in the treatment of liver diseases, specifically HCC.

## Materials and Methods

### Materials

Telmisartan (TLM), a pharmaceutical active agent, was supplied as a free sample from Sigma Pharmaceutical Industries (Menoufia, Egypt). Chitosan polymer (the deacetylation degree = 75–85% and the average molecular weight (Mw) = 100,000–300,000 Da) was purchased from Acros Organics Company (Geel, Belgium). Sodium tripolyphosphate (TPP) as a crosslinking agent, lactose, acetonitrile, methanol (HPLC grade) and dialysis membrane (Mw cut-off 12,000 g/mol) were purchased from Sigma-Aldrich (St Louis, MO, USA). Plastic syringe filter (0.22 µm) and Glacial acetic acid were obtained from Thermo Fisher Scientific (London, UK).

### Methods

#### Synthesis of Lactose-Modified Chitosan

To synthesize LCH, the Maillard reaction (MR) was used, according to a reported method [23]. Briefly, 1 g of each chitosan and lactose was dissolved separately in 50 mL of a 1% (v/v) acetic acid solution (pH 4). Then, the two solutions were added to each other and stirred for 60 h at 70°C and 100 rpm using a hotplate magnetic stirrer. Following that, the reaction was stopped by cooling the mixture for 10 min in an ice bath. The mixture was then neutralized by 1 M NaOH and centrifuged for 15 min at 8000 rpm (Sigma 2–16 KL model, Sigma Laborzentrifugen GmbH, Harz, Germany). The supernatant was purified by dialyzing against 500 mL of deionized water, being replaced daily with fresh deionized water at room temperature for 5 days under continuous magnetic stirring to ensure that all unreacted lactose was completely removed, and then frozen for subsequent freeze-drying. The dry powder was collected, weighed, and stored at room temperature for further characterization.

#### Characterization of Lactose-Modified Chitosan

##### Determination of the Reactive Extent of MR

To measure the reactive extent of MR, a volume of 3 mL was taken every 3 h during the reaction time (60 h) and analyzed utilizing a UV spectrophotometer (Shimadzu UV spectrophotometer, UV-1900i, Japan) by measuring the absorbance at wavelength of 420 nm [24].

### Determination of LCH Solubility

To assess lactose-modified chitosan (LCH) solubility, 50 mg of chitosan and LCH was dissolved in 5 mL of deionized water with vigorous stirring for 5 h, and then filtered through a 0.45-µm filter paper. Following Eq. (1), solubility was calculated gravimetrically based on the change in filter paper weight, which was oven-dried until reaching a constant weight [25].

$$\text{Solubility (g/L)} = \frac{w_0 - w_r}{v} \tag{1}$$

where  $w_0$  represents the initial weight (0.05 g),  $w_r$  represents the retained weight on the filter paper expressed in g, and  $v$  is the volume of the deionized water used, expressed in L (0.005 L).

### Determination of LCH % Yield

The ratio of the lyophilized LCH weight to the combined amount of chitosan and lactose added was used Eq. (2) to calculate the percentage yield of LCH [26].

$$\text{yield (\%)} = \frac{\text{LCH}}{\text{Chitosan} + \text{Lactose}} \times 100 \tag{2}$$

### Fourier Transform Infrared Spectroscopy

FTIR spectra of lactose, chitosan, and lyophilized LCH were examined at a frequency range of 4000 to 400 cm<sup>-1</sup> using a Fourier transform infrared spectroscopy (FTIR) spectrophotometer (FTIR-8300E, Shimadzu, Japan). Samples were grinded with KBr in a constant ratio, and their distinctive bands were detected.

### Determination of the Substitution Degree

The substitution degree (SD%) of the prepared LCH was estimated by calculating the difference between the deacetylation degree (DD%) of LCH and native chitosan according to Eq. (3):

$$\text{SD\%} = \text{DD}_{\text{chitosan}}\% - \text{DD}_{\text{LCH}}\% \tag{3}$$

The DD% of both chitosan and LCH were calculated from their acetylation degree (AD%) according to Eqs. (4) and (5), respectively:

$$\text{DD}_{\text{chitosan}}\% = 100 - \text{AD}_{\text{chitosan}}\% \tag{4}$$

$$\text{DD}_{\text{LCH}}\% = 100 - \text{AD}_{\text{LCH}}\% \tag{5}$$

The AD% of both LCH and chitosan were estimated using Eq. (6), according to a reported method [27].

$$\text{AD\%} = \frac{(A_{1320}/A_{1420}) - 0.03822}{0.03133} \tag{6}$$

where  $A_{1320}$  and  $A_{1420}$  represent the absorption bands of (C-N) and (CH<sub>2</sub>) bending, respectively, which attended from LCH and chitosan FTIR spectra.

## Design and Preparation of TLM-LCH NPs

### Full Factorial Design

A three-factor, two-level (2<sup>3</sup>) full factorial design was performed to optimize the prepared TLM-LCH NPs. Particle size (PS), zeta potential (ZP), and entrapment efficiency (EE) were chosen to be the dependent variables (Table I). TLM amount (A) at two levels (20 and 40 mg), TPP concentration (B) at two levels (1 and 1.25 mg/mL), and LCH concentration (C) at two levels (1 and 2 mg/mL) were selected as the independent variables following a substantial number of preliminary studies. The trials were carried out in all eight combinations (Table II).

### Preparation of TLM-LCH NPs

Eight different formulations according to the above-mentioned design were fabricated following the ionic gelation method first described by [28] with minor changes. After dissolving the LCH in the 20 mL of deionized water, an aliquot of 200 µL of the freshly prepared TLM concentrated solution in glacial acetic acid was added, and a magnetic stirrer was then used to stir the mixture at a speed of 600 rpm for 15 min while the temperature was maintained at room temperature. Then, 8 mL of a TPP solution in deionized water was added dropwise to the TLM-LCH mixture. Subsequent to the addition of the TPP solution, the NPs formed instantaneously. The suspension was stirred for an additional 1 h to promote crosslinking. Afterward, the NPs were placed in a bath sonicator for 10 min before being analyzed. For

**Table I** Coded Units of Levels and Their Matching Variables as Applied in the 2<sup>3</sup> Full Factorial Design

Independent variables	Levels	
	Low	High
A = TLM amount (mg)	20	40
B = TPP concentration (mg/mL)	1	1.25
C = LCH concentration (mg/mL)	1	2
Coded values	-1	+1
Dependent variables	Target	
Y1 = PS	Minimize	
Y2 = ZP	Maximize	
Y3 = EE	Maximize	

**Table II** The Design Matrix of the Prepared TLM-LCH NPs

Formula code	Coded levels			TLM amount (mg)	TPP concentration (mg/mL)	LCH concentration (mg/mL)
	A	B	C			
F1	-1	-1	-1	20	1	1
F2	+1	-1	-1	40	1	1
F3	-1	+1	-1	20	1.25	1
F4	+1	+1	-1	40	1.25	1
F5	-1	-1	+1	20	1	2
F6	+1	-1	+1	40	1	2
F7	-1	+1	+1	20	1.25	2
F8	+1	+1	+1	40	1.25	2

control purposes, drug-free plain NPs were made under the same conditions.

## Characterization of the Prepared TLM-LCH NPS

### Determination of Particle size, Polydispersity Index, and Zeta Potential

The Malvern Zetasizer (Malvern Instruments Ltd. UK), was utilized to assess PDI, PS and ZP of the prepared formulations. Depending on the dynamic light scattering (DLS) method, the PS was investigated. The samples were diluted at a ratio of 1:25 using deionized water, just before each measurement. The electrophoretic light scattering method was used in order to obtain the ZP value.

### Determination of TLM-LCH NPs Entrapment Efficiency

To figure out the EE%, the difference between the free, non-entrapped TLM amount ( $x_2$ ) and the total TLM amount ( $x_1$ ) was calculated according to Eq. (7). The total drug content was obtained by dissolving the polymeric coat after mixing 0.5 mL of the prepared formulation with 1 mL of glacial acetic acid. While, the free TLM was obtained by centrifuging 0.5 mL of the prepared formulation at 15,000 rpm and 4°C for 1 h, followed by separation of the supernatant.

$$EE (\%) = \frac{x_1 - x_2}{x_1} \times 100 \quad (7)$$

The drug amount was determined using a spectrofluorometer (RF-6000 model, Shimadzu, Tokyo, Japan) at an emission wavelength of 365 nm after excitation at 230 [29]. For the concentration range of 20–200 ng/mL, a linear calibration curve was obtained with a correlation coefficient ( $R^2$ ) of 0.9996. As a means of excluding interference from the components of NPs during measurements, plain NPs were employed as a blank.

## Optimization of TLM-LCH NPs Formulations

According to the factorial experimental design, the response optimization method was applied to determine the best conditions for selecting the most optimized formulation using Minitab 19 software. The goal of the optimization procedure was set, which required attaining the lowest possible value for PS while simultaneously reaching the highest possible values for EE and ZP (Table II). After that, the selected formulation was centrifuged, and the NPs were separated before being freeze-dried for additional characterization. Moreover, the optimized formulation's loading efficiency was assessed by calculating the weight of the entrapped drug in NPs per the weight of the NPs.

### Evaluation of the Optimized Formulation

To examine the characteristic bands and rule out the possibility of any interaction between TLM and LCH, the FTIR spectra of TLM, lyophilized blank LCH NPS, and lyophilized optimized TLM-LCH NPs were analyzed using FTIR spectrometer (FTIR-8300E, Shimadzu, Japan). For examining the morphological characteristics of the optimized formulation, a transmission electron microscope (TEM) (model 2100, JEOL®, Tokyo, Japan) was used.

### In Vitro TLM Release Study

The *in vitro* release study of TLM-LCH NPs was conducted utilizing the dynamic dialysis method [30]. The dialysis membrane was immersed overnight in phosphate buffer saline (PBS) pH 7.4 to guarantee full swelling. An aliquot of 0.5 mL (equivalent to 1 mg TLM) of each TLM-LCH NPs, TLM-NPs, and plain TLM suspended in PBS pH 7.4 was inserted into the dialysis bag and then submerged into the release medium (150 mL PBS pH 5.5 or 7.4) with stirring at 100 rpm and 37°C. For 24 h, samples of 3 mL were withdrawn at certain time points, and replaced with a 3-mL of fresh buffer. The TLM amount

released was quantified spectrofluorimetrically at an emission wavelength of 365 nm. The % cumulative TLM release was determined using Eq. (8).

$$\% \text{ cumulative TLM release} = \frac{Q_t}{Q_0} \times 100 \quad (8)$$

where,  $Q_t$  represents the amount of TLM that has been released at time  $t$  and  $Q_0$  is the TLM amount that was added initially.

### Release Kinetics

The TLM release data were analyzed kinetically utilizing DDSolver for Microsoft Excel software. The release data of TLM-LCH NPs was fit into the following models: Higuchi (Eq. (9)), first-order (Eq. (10)), zero-order (Eq. (11)), and Korsmeyer-Peppas (Eq. (12)) [31]. The model with the highest  $R^2$  value will be the most optimal release kinetics model.

$$Q_t/Q_0 = K_H \sqrt{t} \quad (9)$$

$$Q_t = Q_0(1 - e^{-K_1 t}) \quad (10)$$

$$Q_t/Q_0 = K_0 t \quad (11)$$

$$Q_t/Q_0 = K_{KP} t^n \quad (12)$$

where  $K_H$  is the Higuchi constant,  $K_1$  is the first-order release constant,  $K_0$  is the zero-order release constant,  $K_{KP}$  is a Korsmeyer-Peppas constant, and the release exponent ( $n$ ) represents the TLM release mechanism, where Fickian diffusion release for  $n \leq 0.45$  and non-Fickian release (anomalous) for  $0.45 < n < 0.89$ , indicates that drug release was maintained by erosion and diffusion together. When  $n$  is greater than 0.89, it is associated with zero order release, in which drug release is almost entirely owing to particle erosion [32].

### Effect of Storage

To evaluate the influence of storage on the physical properties of the lyophilized optimized formulation, the lyophilized powder was packed into brown glass vials and stored under different storage circumstances for 6 months at 4°C and ambient temperature (TA). The optimized formulation was examined for different parameters, including PS, PDI, ZP, and TLM encapsulation. Prior to each measurement, the stored samples were reconstituted with PBS (pH 7.4) and sonicated for 5 min.

### Liver Targeting Efficiency

The efficiency of the optimized formulation in targeting the liver was assessed by determining the ratio of the TLM-liver concentration to the TLM-plasma concentration ( $C_{liver}/C_{plasma}$ ) at three distinct time intervals: 2, 4, and 8 h. Twenty-seven male Wister rats (220–240 g) were randomly divided into 3 groups of 9 rats each. All rats were housed and received similar diet. The study was conducted according to the worldwide guidelines for the Care and Use of Laboratory Animals and were authorized by the Research Ethics Committee of Faculty of Pharmacy, Tanta University (Protocol NO. PT-0092). The three TLM treatments (Plain TLM, TLM-NPs, and TLM-LCH NPs dispersed in PBS pH 7.4) were intraperitoneally administered to the rats of the first, second, and third groups, respectively at TLM-dose equivalent to 10 mg/Kg [33]. At each time interval, blood samples were collected from 3 rats of each group and centrifuged at 3000 rpm for 10 min to separate plasma. After collecting blood samples, the rats were euthanized by cervical dislocation and dissected to separate liver. Following that, the liver was precisely weighed and homogenized after adding 10 mL of acetonitrile using the Ultra Turrax homogenizer (IKA, Werke GmbH & Co. KG, Germany). Plasma samples and liver homogenates were kept frozen at -80°C until being assayed using a reported spectrofluorometric method [29].

### Statistical Analysis

Minitab 19 statistical software was utilized to determine the statistical analysis for the factorial design. Multiple regression analysis was conducted to evaluate the response as described by the following polynomial Eq. (13):

$$Y = b_0 + b_1 A + b_2 B + b_3 C + b_{12} AB + b_{23} BC + b_{13} AC + b_{123} ABC \quad (13)$$

where,  $Y$  is the dependent response,  $b_0$  is the mathematical average response from all runs, and  $b_x$  is the calculated coefficient for the independent variable  $x$ . The mean effect (A, B, and C) represents the average outcome of elevating one element from a low to high level at a time. While AB, BC, AC, and ABC are the interaction terms that demonstrate how the response varies when modifications are applied to two distinct factors simultaneously.

The other findings were statistically analyzed using GraphPad Prism 6 Software, which used the t-test to assess the statistical significance of the difference between the mean values of two groups. While for comparing various groups, the one-way ANOVA followed by the Tukey–Kramer multiple comparison test was utilized.



The obtained results were reported as (mean  $\pm$  SD), and a  $p$ -value  $< 0.05$  showed a statistically significant difference.

## Results and Discussion

### Synthesis of LCH

Chitosan can be modified via a variety of techniques, such as amide bond formation, reductive N-alkylation, and glycation [34]. However, MR was chosen to be the method for LCH preparation as it is simple with fewer steps and safe compared to the other methods. MR occurs without using coupling agents or reducing agents such as sodium cyanoborohydride, which is known for its toxicity [35].

### Characterization of LCH

#### Determination of the Reactive Extent of MR

By measuring the UV absorbance at  $\lambda$  420 nm, the last stages of the MR were detected. As illustrated in Fig. 1, spectroscopy demonstrated a rise in absorbance at wavelength of 420 nm as a function of time, indicating the development of colorful end products. The brownish-colored reaction medium made this clear. Our findings indicate that lactose was successfully attached to the chitosan backbone. Previous studies revealed a similar manner during absorbance measurement at 420 nm [23, 36].

#### Determination of LCH Solubility

Chitosan is insoluble at neutral or high pH; however, it is soluble in formic and acetic acids, which have limited pharmaceutical applications. In this study, the solubility of

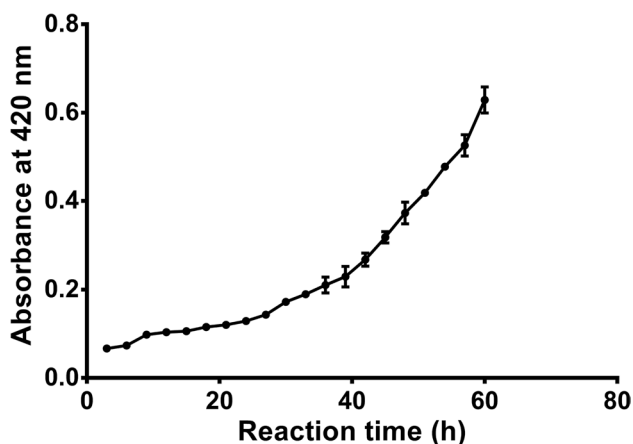


**Fig. 1** The reactive extent of the Maillard reaction between chitosan and lactose during 60 h. Data are represented as mean  $\pm$  SD,  $n = 3$

LCH in deionized water ( $6.28 \pm 0.21$  g/L) was significantly ( $p < 0.05$ ) higher solubility than that of native chitosan ( $0.25 \pm 0.03$  g/L). These results correlate with previous studies [23, 24]. The crystalline structure of chitosan and the presence of amino group, or acetamide residues, are crucial for the production of irregular conformational forms via intramolecular hydrogen bonding, which promotes polymer aggregation and low solubility [37]. However, chitosan's solubility can be improved by incorporating a hydrophilic molecule like lactose and eliminating two hydrogen atoms from its amino groups.

#### Determination of LCH % Yield

In terms of % yield, the prepared LCH amount to initial added amount ratio was  $0.877 \pm 0.011$  g to 2 g (1 g chitosan + 1 g lactose), resulting in a yield of  $43.85 \pm 0.56\%$  which is considered a good yield given that the LCH concentration used in NPs formulations was 1–2 mg/mL.

#### Fourier Transform Infrared Spectroscopy

The attachment of lactose to the chitosan backbone was confirmed by FTIR spectroscopy. Figure 2 shows the obtained FTIR spectra for lactose (a), chitosan (b), and LCH (c). The FTIR spectrum of lactose showed the existence of carbonyl groups in a band at  $1651$   $\text{cm}^{-1}$ , which disappeared in the LCH spectrum, indicating the participation of the lactose carbonyl group in the reaction with the chitosan amino group to create Schiff base.

The FTIR spectrum of LCH was found to be distinct from that of native chitosan, proving that lactose had been incorporated into the polymer backbone. The first and most

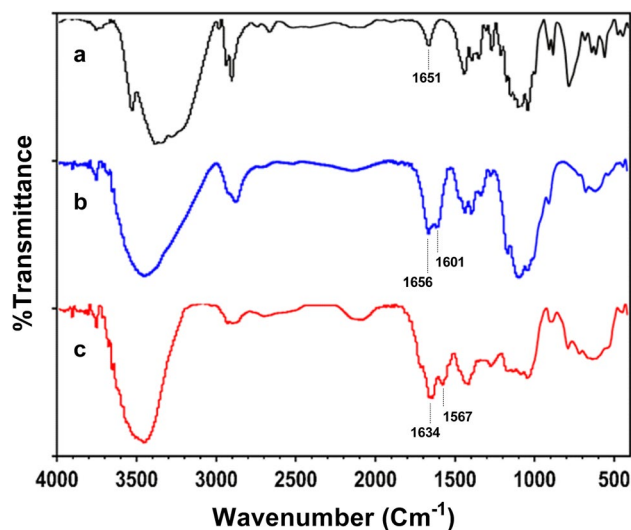


**Fig. 2** FTIR spectra of lactose (a), chitosan (b), and LCH (c)

**Table III** The Characterization Results (Mean ± SD, *n* = 3) of the Prepared TLM-LCH NPs in the Applied 2<sup>3</sup> Factorial Design

Formula	EE %	PS (nm)	PDI	ZP (mV)
F1	90.45 ± 0.67	144.16 ± 1.51	0.13 ± 0.024	27.1 ± 0.56
F2	77.31 ± 1.07	256.15 ± 2.15	0.304 ± 0.086	21.73 ± 1.01
F3	81.05 ± 0.18	115.26 ± 1.91	0.245 ± 0.038	23.7 ± 0.81
F4	73.56 ± 0.49	195.7 ± 3.4	0.289 ± 0.091	15.56 ± 0.305
F5	83.82 ± 0.58	405.76 ± 7.8	0.288 ± 0.035	35.5 ± 1.57
F6	92.9 ± 0.39	466.73 ± 1.96	0.268 ± 0.055	37.8 ± 0.265
F7	83.86 ± 1.05	270.26 ± 2.49	0.269 ± 0.044	28.36 ± 0.351
F8	91.71 ± 0.8	362.33 ± 5.53	0.194 ± 0.069	27.25 ± 0.252

important indicator for the chitosan modification is that, the shift in the amide I band from 1656 cm<sup>-1</sup> in chitosan to 1634 cm<sup>-1</sup> in LCH, as marked in the figure, revealing the creation of -C = N bonds, typical of Schiff bases formed during MR. Additionally, the amide II band, previously located at 1601 cm<sup>-1</sup>, migrated to 1567 cm<sup>-1</sup> and became more intense.

The second distinction is that LCH spectrum showed more pronounced variations between 1400 and 500 cm<sup>-1</sup> than those of native chitosan spectrum. This area is unique to saccharide structure, and this increase is related to the increase in number of CH<sub>2</sub> groups resulted from the incorporation of the lactose chain into the chitosan [38, 39]. These findings confirm the incorporation of lactose molecules onto the structural backbone of chitosan through the MR.

**Determination of the SD%**

The DD% of chitosan and LCH were found to be 79.384% and 65.049%, respectively. After calculating the difference between them the SD% was found to be 14.335%. The generated SD% made is perfect for the study’s goal, which is to

target hepatocytes, because Kupffer cells also have galactose receptors distinct from ASGPR [40]. The galactose residue in lactose is a ligand for both receptors. However, the level of lactosylation affects selectivity. Receptors on Kupffer cells preferred higher lactosylation degree (50% or more), while the ASGPR on hepatocytes took up NPs with lower lactosylation degree [41, 42]. Therefore, it is important to maintain a reasonable galactose density to avoid a switch from hepatocytes to the receptors of Kupffer cells.

**Characterization of TLM-LCH NPs**

**Size Distribution of the Prepared TLM-LCH NPs**

Table III displays the mean PS in a nanometric range as well as the PDI values for each formulation. The generated PS ranges from 115.26 ± 1.91 nm to 466.73 ± 1.96 nm, and the PDI values varied from 0.13 ± 0.024 to 0.304 ± 0.086, demonstrating a relatively uniform size distribution with good physical stability [43]. According to these findings, the PS range of the produced TLM-LCH NPs is optimal for the study’s goal of liver targeting, as the diameter of fenestrae in normal liver sinusoids is around 50–200 nm [44]. NPs with sizes smaller than 200 nm can infiltrate through sinusoids [45]. This allows NPs to evade Kupffer cell capture and reach hepatocytes, due to the fact that macrophages participate in the removal of particles with a diameter greater than 0.5 μm [46].

Equation (14) describes the regression analysis to examine the association between Y1 (PS) and the independent variables.

$$PS = 277.05 + 43.183A - 41.185B + 99.225C - 0.058AB - 4.925AC - 18.817BC + 7.833ABC \tag{14}$$

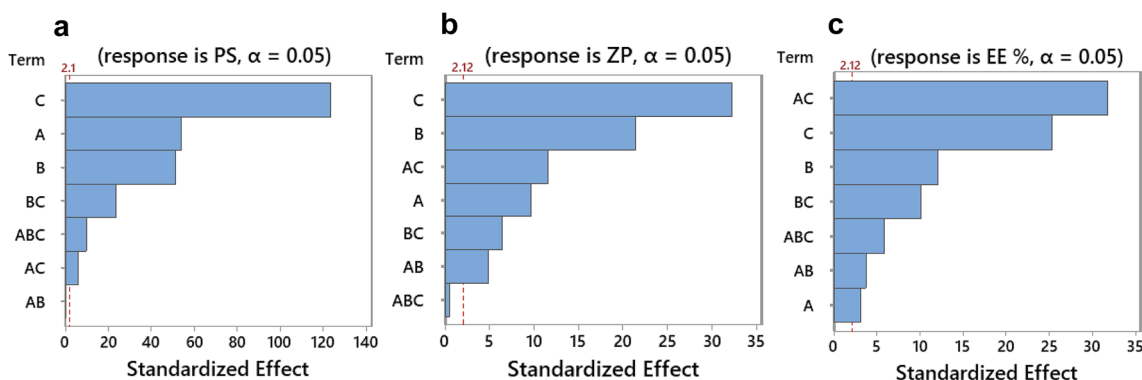


**Fig. 3** Pareto charts of standardized effects on (a) PS, (b) ZP, and (c) EE. The red dashed line represents a reference line for statistical significance depends on the significance level (denoted by α = 0.05).

A, B, and C factors stand for TLM concentration, TPP concentration, and LCH concentration, respectively. The interaction terms for the three factors are represented by AB, BC, AC, and ABC

According to the regression analysis and Pareto chart (Fig. 3a), all factors with the exception of AB ( $p = 0.943$ ) significantly impacted PS ( $p < 0.05$ ). The most significant factor was LCH concentration (+C), the positive coefficient value implies that increasing the amount of LCH considerably increases PS. The increase in PS with increasing LCH concentration could be due to the increase in the polymer particles generating each vesicle, as there is a direct relationship between vesicle size and number of particles [43, 47].

The second factor was TLM amount (+A), indicating that higher levels of TLM content led to PS enlargement. This is a common occurrence in Chitosan-TPP NPs [48]. This is most likely owing to the entrapped drug Mwt contribution to the increase in PS. Based on these findings, the optimal formulation conditions for PS were found to be 1.25 mg/mL TPP, 20 mg TLM, and 1 mg/mL LCH, which correspond to the F3 ( $115.26 \pm 1.91$  nm). The response surface plots and contour plots that demonstrate graphically the effect of the factors on the PS are shown in Fig. 4.

#### Zeta Potential of the Prepared TLM-LCH NPs

Table III displays the mean ZP in millivolt unit (mV). The obtained values of ZP ranged from  $+15.56 \pm 0.305$  mV to  $+37.8 \pm 0.265$  mV with a positive charge for all

generated TLM-LCH NPs, the (+NH<sub>3</sub>) groups on the surface of the NPs were thought to be the cause of this charge. The positive charge is optimal for liver targeting, as the charge on NPs' surfaces has an impact on their cellular internalization. Hepatocytes have a greater affinity for positively charged NPs [49, 50], whereas negatively charged NPs are ingested by Kupffer cells [51].

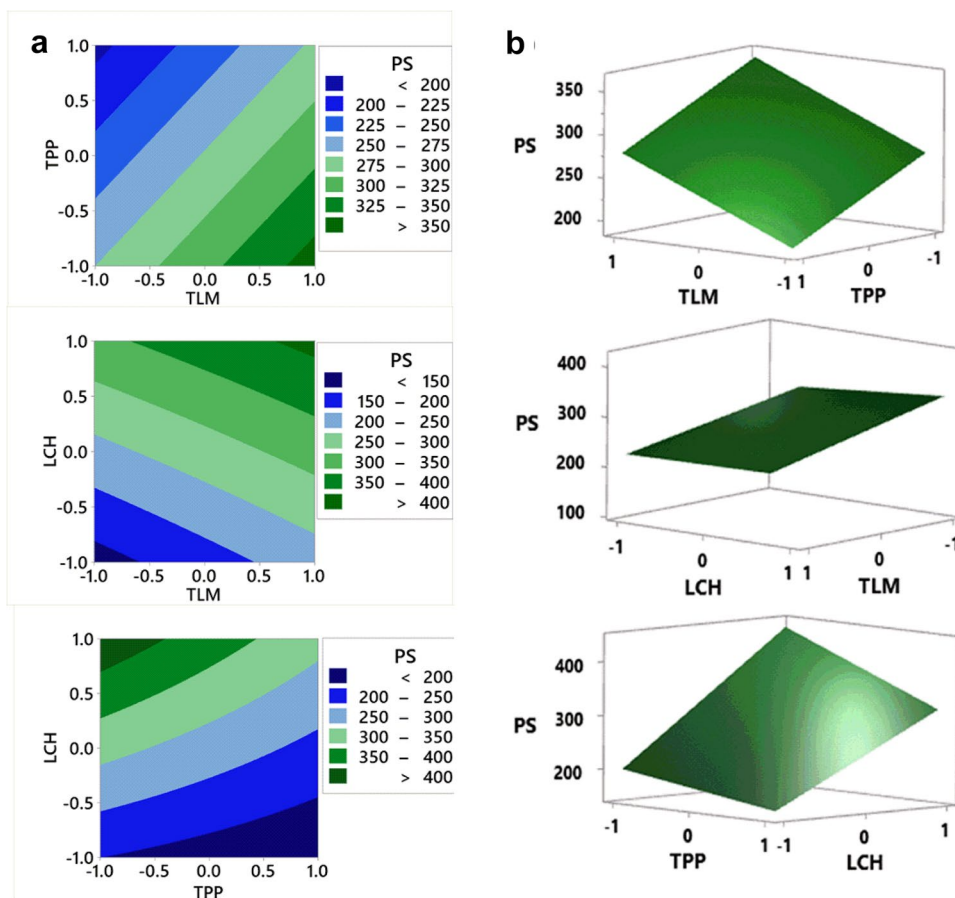
The regression analysis that describes the association between the independent variables and Y2 (ZP) is reported in Eq. (15).

$$ZP = 27.125 - 1.533A - 3.400B + 5.108C - 0.775AB - 1.017BC + 1.833AC - 0.075ABC \quad (15)$$

According to the Pareto chart (Fig. 3b) and regression analysis, all factors exhibited significant effects ( $p < 0.05$ ) on ZP except for interaction ABC ( $p = 0.643$ ). LCH concentration (+C) was the most effective factor, indicating a direct relationship between polymer concentration and ZP value. This could be attributed to an increase in positively charged amino groups in LCH as polymer concentration increases.

The second effective factor was TPP concentration (-B), indicating that there is an inverse relation between TPP concentration and ZP value. This behavior can be related to the more negatively charged phosphate ions

**Fig. 4** The contour plots (a) and response surface plots (b) for the PS with variances of TLM, TPP, and LCH





accompanied by higher TPP concentrations, which react with the positively charged (NH<sub>3</sub>) groups of chitosan, resulting in a reduction in the positive charge. The third effective component was + AC which is provided in formulations F1, F3, F6, and F8. But with its combination of +C and -B, F6 emerged as the most optimal in terms of zeta potential (+ 37.8 ± 0.265 mV). The response surface and contour plots that demonstrate graphically the impact of the selected factors on the ZP are shown in Fig. 5.

**The Entrapment Efficiency of the Prepared TLM-LCH NPs**

The mean EE of the prepared formulations ranged from 73.56 ± 0.49% to 92.9 ± 0.39%. The regression analysis for the response Y3 (EE) is reported in Eq. (16).

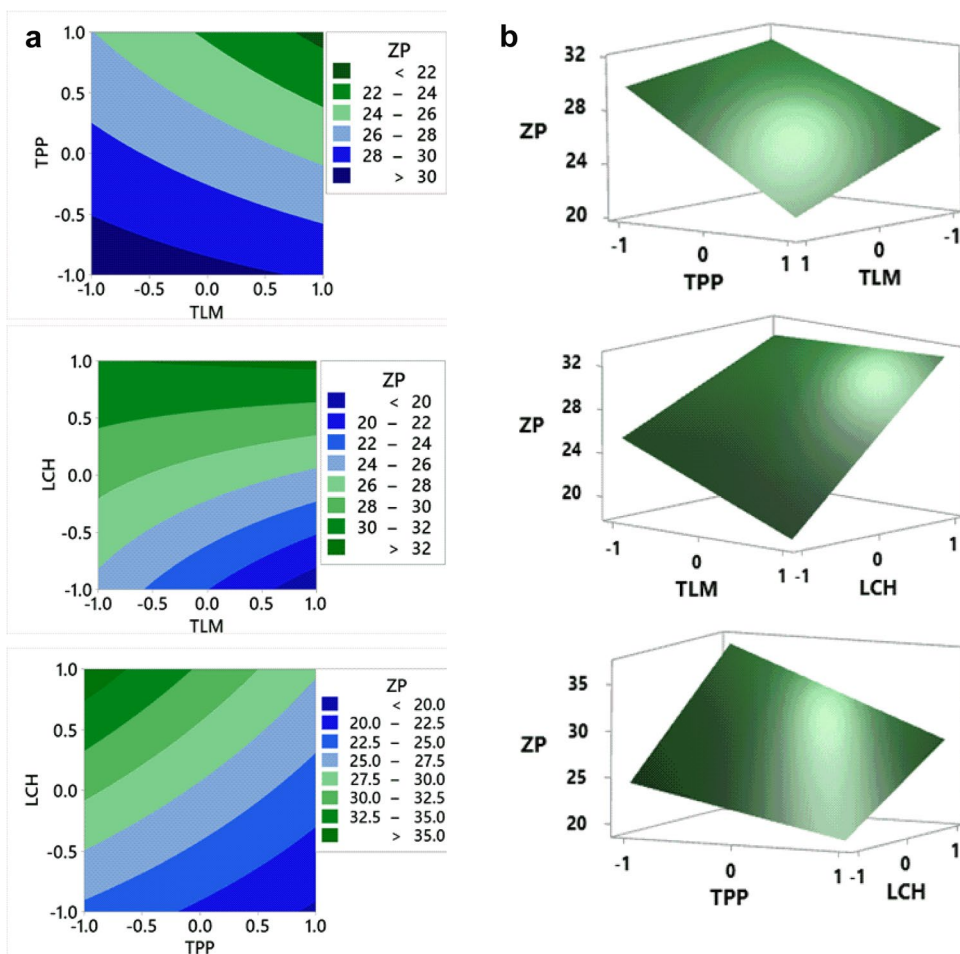
$$EE = 84.334 - 0.463A - 1.787B + 3.739C + 0.551AB + 4.695AC + 1.500BC - 0.859ABC \quad (16)$$

In accordance with the regression equation and Pareto chart (Fig. 3c), all parameters had substantial effects (*p* < 0.05) on the EE %. The most significant factor was the interaction between TLM amount and LCH concentration

(+ AC), which showed that a rise in the EE % is achieved by raising both variables simultaneously. The second significant factor was (+C), which showed that adding more LCH led to a notable improvement in the EE%. We can infer from (- B), the third efficient factor, that there is a rise in EE % with the decrease in TPP concentration. According to these findings, 2 mg/mL LCH, 40 mg TLM, and 1 mg/mL TPP provide the best formulation conditions for EE %, which is F6 (92.9 ± 0.39%).

The increase in EE% with increasing polymer content could be explained as follows: the higher the polymer content, the more polymer particles create each vesicle, and the higher the EE% of the drug. Another explanation is that the electrostatic interaction between free amino groups of LCH and the carboxylic groups of TLM, which is confirmed by FTIR, resulted in an improvement in the EE%. As LCH content increased, so did the number of amino and hydroxyl groups accessible for interactions with TLM, improving encapsulation efficiency. In many prior investigations, raising the drug’s concentration with chitosan resulted in much better drug encapsulation, which was attributed to the drug’s ionic interaction with chitosan [52, 53]. The response surface

**Fig. 5** The contour plots (a) and response surface plots (b) of the ZP with variances of TLM, TPP, and LCH



and contour plots that demonstrate graphically the impact of the selected factors on the EE % are shown in Fig. 6.

### Optimization of TLM-LCH NPs

After application of the response optimization method, the optimization plot (Fig. 7) indicates that, the optimized formulation concerning all the measured parameters was (F1), which contains 20 mg TLM, 1 mg/mL TPP, and 1 mg/mL LCH. The lyophilized optimized formulation (F1) displayed a PS of  $145.46 \pm 0.7$  nm, a PDI of  $0.148 \pm 0.05$ , a loading efficiency of  $21.68 \pm 0.89\%$ , an EE % of  $90.21 \pm 0.28\%$ , and a ZP of  $+27.13 \pm 0.21$  mV.

### Fourier Transform Infrared Spectroscopy

Figure 8 shows the FTIR spectra of TLM, blank LCH NPs, and TLM-LCH NPs. After loading the NPs with the drug, a reduction in the peak intensity of the chitosan (NH<sub>2</sub>) group at  $1657\text{ cm}^{-1}$  was observed. Also, the carboxyl group absorption peak of TLM at  $1700\text{ cm}^{-1}$  disappeared, and a new peak was developed at  $1566\text{ cm}^{-1}$ , related to the N–H vibrations in amide (CONH), which confirmed the

interaction between TLM and LCH via the amide bond [22, 54]. Furthermore, the spectra of TLM-LCH NPs differed significantly from the spectra of pure TLM NPs, whereas there are no discernible differences in the spectra profiles of blank NPs and TLM-LCH NPs. This might be because of the extremely low concentrations of loaded TLM on the NPs' surfaces, or it could be because the TLM is mainly embedded in the NPs' matrices, both of which are consistent with the high EE %.

### Morphology of the Optimized TLM-LCH NPs Formulation

Using TEM, the morphological characters of the prepared TLM-LCH NPs were investigated (Fig. 9). TEM analysis showed that all of the NPs were nanometer-sized, with a narrow size distribution, and nearly spherical in shape; this is advantageous for cellular uptake because, as previously mentioned, spherical particles are taken up more readily than rod-shaped ones due to the longer membrane wrapping time required for the latter [55]. Additionally, the lack of aggregation and disruptions emphasized the vesicle's integrity. It is worth noting here that the PS determined by DLS analysis was larger than that obtained from TEM micrographs.

**Fig. 6** The contour plots (a) and response surface plots (b) of the EE with variances of TLM, TPP, and LCH

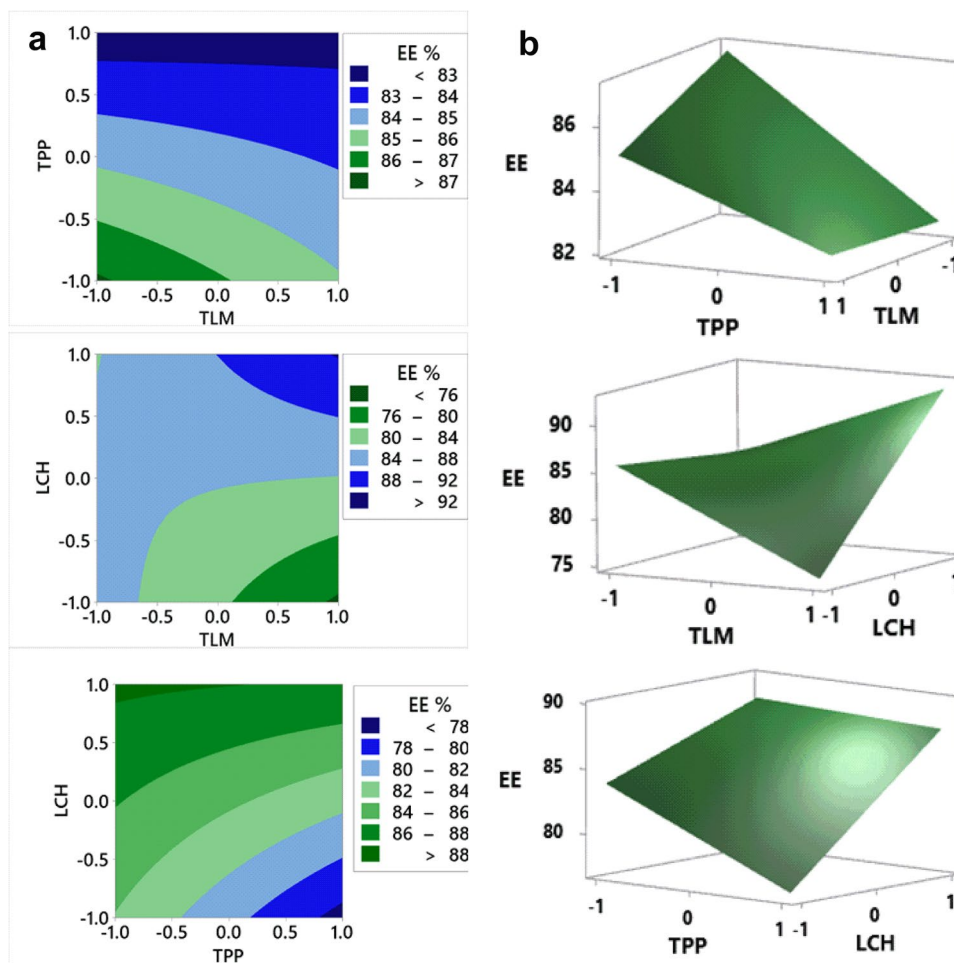
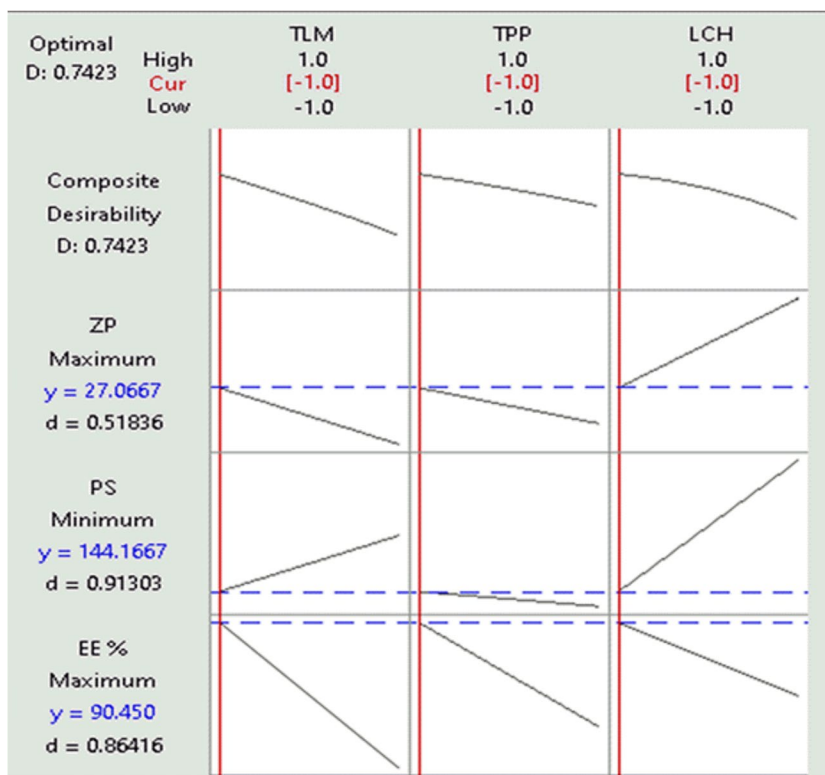


**Fig. 7** The response optimization plot of Minitab. The vertical red lines represent the current factor settings. The numbers displayed in red at the top of a column show the current factor level settings. The horizontal blue lines and numbers represent the responses for the current factor level



Hydrodynamic particle diameter is calculated using the DLS, which is a multi-angle measuring approach. However, the actual diameter of the particle is determined by the TEM experiment [56].

**In Vitro TLM Release Study**

Both the extracellular physiological pH of 7.4 and the tumor cell microenvironment pH of 5.5 were used to assess the *in vitro* release of plain TLM, TLM-loaded unmodified NPs

(TLM-NPs), and TLM-LCH NPs. As illustrated in Fig. 10, at both pH, the % cumulative of TLM release from both LCH and unmodified NPs formulations showed a significant increase ( $p < 0.05$ ) compared to the plain drug suspension. At pH 7.4, the % cumulative of TLM release from LCH and unmodified NPs within 24 h were  $32.39 \pm 1.69\%$  and  $43.28 \pm 3.3\%$ , respectively, while it was  $15.98 \pm 2.11\%$  from

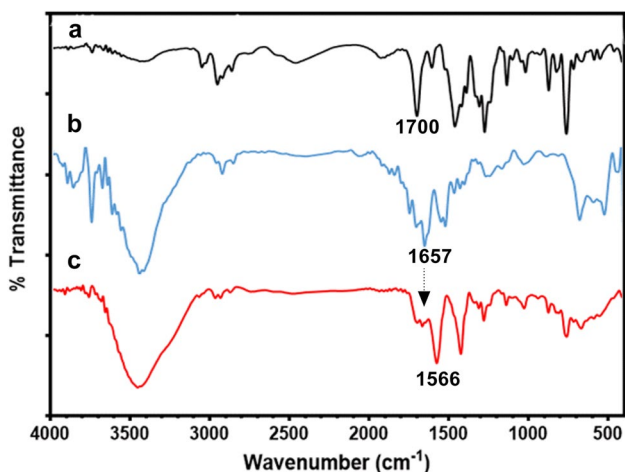


**Fig. 8** FTIR spectra of TLM (a), blank NPs (b), and TLM-LCH NPs (c)

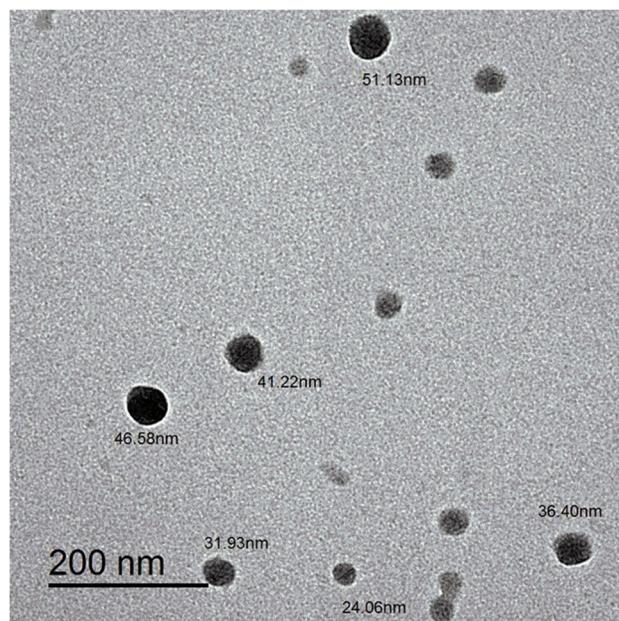


**Fig. 9** TEM of the optimized formulation



plain TLM suspension (Fig. 10a). This may be attributable to the developed nanosized particles [57]. As the smaller the PS, the larger the surface area, this gives more space to retain the drug, leading to TLM solubilization and a significant enhancement in drug release. In contrast, TLM suspension showed a lower drug release, which was previously explained by the fact that TLM is crystalline [58] and that its solubility is pH-dependent, with a maximum solubility being reached under strongly acidic (pH < 3) or basic conditions (pH > 9), but being insoluble in the pH range of 3–9 [59].

Regarding the release pattern of TLM-LCH NPs and TLM-NPs, both formulations demonstrated biphasic drug release, with an initial burst of TLM within the first 3 h, followed by a steady release of the drug. The initial rapid release may be caused by the TLM, which are loosely integrated on the surface of the NPs by an amide bond [60]. Moreover, the TLM-LCH NPs formulation showed a lower drug release profile compared to TLM-NPs. This may be because of the lactose coating on the NPs' surface, which slows the TLM release.

The most interesting observation is that LCH NPs demonstrated significantly ( $p < 0.05$ ) higher release at pH 5.5 compared to pH 7.4, indicating a greater release upon reaching the tumor microenvironment and hence increasing the drug concentrations within HCC. The enhanced drug release at pH 5.5 may be explained by the fact that chitosan exhibits a swelling characteristic in acidic pH conditions [22].

After fitting the release data results of the TLM-LCH NPs into the mentioned mathematical models, the  $R^2$  value was found to be maximum for the Higuchi model at both pH (Table IV). Furthermore, the  $n$  exponent values at pH 7.4 and pH 5.5 were  $0.369 \pm 0.044$  and  $0.626 \pm 0.053$ , respectively. These results revealed that the TLM release from LCH NPs at pH 7.4 followed Fickian diffusion, meaning that the drug release was controlled mainly by diffusion. At pH 5.5, however, non-Fickian release (anomalous) was observed, indicating that drug release was maintained by both erosion and diffusion. These findings revealed a slow TLM release rate for LCH NPs, and its release would be controlled mainly by diffusion within the blood circulation conditions. However, a higher release controlled by diffusion and polymer erosion

**Table IV** Mathematical Models and Parameters of the Release Study of TLM-LCH NPs at pH 5.5 and pH 7.4, (Mean  $\pm$  SD,  $n=3$ )

Release model	Release medium pH	
	pH 5.5	pH 7.4
Zero-order	$R^2=0.9529 \pm 0.007$	$R^2=0.8677 \pm 0.025$
First-order	$R^2=0.9870 \pm 0.002$	$R^2=0.8789 \pm 0.011$
Higuchi	$R^2=0.9947 \pm 0.006$	$R^2=0.9581 \pm 0.005$
Korsmeyer-Peppas	$R^2=0.9962 \pm 0.003$	$R^2=0.9740 \pm 0.004$
	$n=0.626 \pm 0.053$	$n=0.369 \pm 0.044$

will be obtained upon reaching the tumor cells and even after cellular internalization via receptor-mediated endocytosis in lysosomes or endosomes, which have pH 4.5–5 and pH 5.5–6, respectively [61], highlighting the potential of TLM-LCH NPs as an effective therapy for HCC.

### Effect of Storage

The optimized formulation F1 displayed acceptable physicochemical changes (Table V), as no significant difference ( $p > 0.05$ ) was detected in the measured parameters, except for PS, which increased significantly ( $p = 0.022$ ) after 6 months of storage at TA. The increase in PS may be resulted from the particles' aggregation and the swelling nature of chitosan [62, 63]. Furthermore, the changes in the evaluated parameters were found to be the least at 4°C when compared to the formulation stored at TA. Based on these results, it has been shown that the optimized formulation is better stored as a lyophilized powder under refrigerated conditions to attain a greater degree of stability and prevent the aggregation of NPs.

### Liver Targeting Efficiency

Figure 11 represents the results of the efficiency of the TLM-LCH NPs in targeting the liver compared to plain TLM and TLM-NPs at three distinct time intervals: 2, 4, and 8 h. According to the obtained data, after the first 2 h, plain TLM showed a higher  $C_{liver}/C_{plasma}$  ratio compared

**Fig. 10** The mean cumulative % of TLM release ( $\pm$  SD,  $n=3$ ) from TLM-NPs, TLM-LCH NPs, and plain TLM at (a) pH 7.4 and (b) pH 5.5

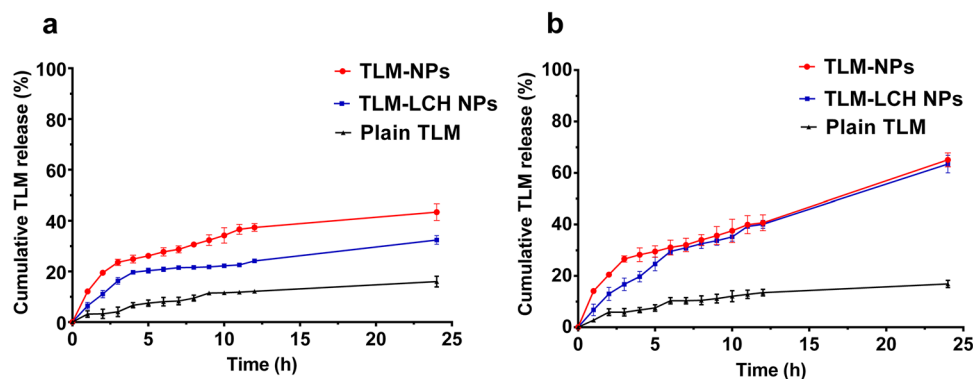


**Table V** The Effect of Storage on the Optimized Formulation During Storage for 6 Months at Ambient Temperature and 4°C. Values Are Represented as Mean ± SD, n = 3

Storage conditions		Evaluation parameters			
		PS(nm)	PDI	ZP(mV)	EE%
Initial		145.46 ± 0.7	0.148 ± 0.053	27.13 ± 0.21	90.21 ± 0.28
1 <sup>st</sup> month	4°C	146.2 ± 0.88	0.168 ± 0.056	26.9 ± 0.26	90.02 ± 0.92
	TA	147.03 ± 0.97	0.174 ± 0.058	26.2 ± 1.13	89.13 ± 1.01
2 <sup>nd</sup> month	4°C	146.93 ± 1.01	0.191 ± 0.032	26.66 ± 1.06	89.45 ± 0.49
	TA	149.27 ± 1.67	0.205 ± 0.055	26.41 ± 1.27	86.83 ± 2.3
3 <sup>rd</sup> month	4°C	147.8 ± 1.25	0.204 ± 0.006	26.13 ± 0.86	89.18 ± 1.53
	TA	150.33 ± 4.12	0.241 ± 0.059	24.9 ± 0.85	86.18 ± 1.78
6 <sup>th</sup> month	4°C	152.1 ± 3.47	0.265 ± 0.041	25.8 ± 0.56	86.95 ± 2.14
	TA	160.76 ± 4.69	0.334 ± 0.122	24.46 ± 1.71	83.95 ± 2.82

to the unmodified NPs. This may attributed to the rapid hepatic absorption of TLM by hepatic organic anion transporter polypeptide that increase the initial liver concentration [64] combined with the lower plasma concentration at that time due to the limited aqueous solubility of TLM. However, there was a significant ( $p < 0.05$ ) increase in the Cliver/Cplasma ratio of TLM-LCH NPs at the all-selected time intervals compared to the other formulations, as the  $C_{liver}/C_{plasma}$  ratio was nearly 2- to threefold that observed in case of plain TLM and 1.5- to twofold that observed in case of unmodified TLM-NPs. The obtained results reflected the high targeting ability of the TLM-LCH NPs. The higher  $C_{liver}/C_{plasma}$  ratio for TLM-LCH NPs compared to plain TLM and TLM-NPs may be related to the presence of lactose molecules, which act as an active-targeting ligand, ensuring a high, selective binding affinity for the ASGPR of hepatocytes and allowing NPs to be internalized intracellularly via receptor-mediated endocytosis.

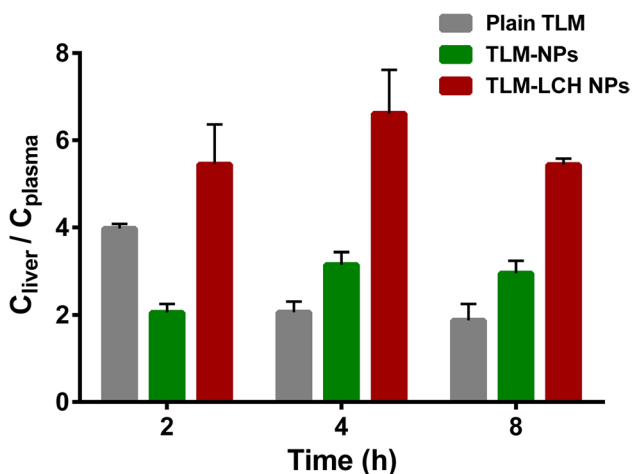


**Fig. 11** Liver targeting efficiency of the TLM-LCH NPs compared to plain TLM and TLM-NPs by measuring the TLM-liver concentration to the TLM-plasma concentration ratio ( $C_{liver}/C_{plasma}$ ) at three distinct time intervals: 2, 4, and 8 h (mean ± SD, n = 3)

### Conclusion

In conclusion, LCH was successfully synthesized via MR and demonstrated its potential as a liver- targeted nanocarrier for TLM. The established factorial design allowed for the successful preparation of TLM-LCH NPs with reasonable physicochemical characteristics via optimization of the parameters involved in the ionic gelation method. The optimized formulation showed a better stability after being stored as a lyophilized powder for 6 months at 4°C, while at ambient temperature, a notable rise in PS was observed. *In vitro* release study exhibited that the prepared TLM-LCH NPs were stable at circulation pH with a controlled rate of release, while at acidic tumor pH, the drug release was faster due to polymer swelling and erosion. Additionally, liver targeting efficiency study revealed that, TLM-LCH NPs exhibited a significant increase ( $p < 0.05$ ) in the  $C_{liver}/C_{plasma}$  ratio compared to plain TLM and unmodified TLM-NPs. All of these characteristics point to the high potential of the prepared TLM-LCH NPs for increasing TLM distribution into liver tissues, which could improve its efficacy when used to treat HCC.

**Acknowledgements** The authors are grateful to Dr. Mona Hamdy from Drug Analysis and Chromatography lab for her technical support. In addition, we would like to thank the Nanotechnology lab in Delta University for Science and Technology for material characterization.

**Author Contribution** Mohamed Nasr: Conceptualization, formal analysis, supervision, writing – reviewing and editing. Sanaa A. El-Gizawy: Conceptualization, supervision, data curation, validation and visualization. Ebtessam A. Essa: Conceptualization, supervision, writing – reviewing and editing. Ahmed Y. Kira: Conceptualization, investigation, methodology, writing and reviewing. Sameh Saber: Conceptualization, material preparation, data collection and analysis.

**Funding** Open access funding provided by The Science, Technology & Innovation Funding Authority (STDF) in cooperation with The Egyptian Knowledge Bank (EKB).



## Declarations

**Conflict of Interest** The authors declare no competing interests.

**Open Access** This article is licensed under a Creative Commons Attribution 4.0 International License, which permits use, sharing, adaptation, distribution and reproduction in any medium or format, as long as you give appropriate credit to the original author(s) and the source, provide a link to the Creative Commons licence, and indicate if changes were made. The images or other third party material in this article are included in the article's Creative Commons licence, unless indicated otherwise in a credit line to the material. If material is not included in the article's Creative Commons licence and your intended use is not permitted by statutory regulation or exceeds the permitted use, you will need to obtain permission directly from the copyright holder. To view a copy of this licence, visit <http://creativecommons.org/licenses/by/4.0/>.

## References

- Asrani SK, Devarbhavi H, Eaton J, Kamath PS. Burden of liver diseases in the world. *J Hepatol*. 2019;70(1):151–71. <https://doi.org/10.1016/j.jhep.2018.09.014>.
- Stepanova M, De Avila L, Afendy M, Younossi I, Pham H, Cable R, et al. Direct and indirect economic burden of chronic liver disease in the United States. *Clinical Gastroenterology and Hepatology*. 2017;15(5):759–66. e5. <https://doi.org/10.1016/j.cgh.2016.07.020>.
- Devan AR, Nair B, Kumar AR, Nath LR. An insight into the role of telmisartan as PPAR- $\gamma/\alpha$  dual activator in the management of nonalcoholic fatty liver disease. *Biotechnol Appl Biochem*. 2022;69(2):461–8. <https://doi.org/10.1002/bab.2123>.
- Fujita K, Yoneda M, Wada K, Mawatari H, Takahashi H, Kirikoshi H, et al. Telmisartan, an angiotensin II type 1 receptor blocker, controls progress of nonalcoholic steatohepatitis in rats. *Dig Dis Sci*. 2007;52(12):3455–64. <https://doi.org/10.1007/s10620-007-9741-4>.
- Abdelhamid AM, Elsheakh AR, Suddek GM, Abdelaziz RR. Telmisartan alleviates alcohol-induced liver injury by activation of PPAR- $\gamma$ /Nrf-2 crosstalk in mice. *International Immunopharmacology*. 2021;99:107963. <https://doi.org/10.1016/j.intimp.2021.107963>.
- Saber S, Khodir AE, Soliman WE, Salama MM, Abdo WS, Elsaed B, et al. Telmisartan attenuates N-nitrosodiethylamine-induced hepatocellular carcinoma in mice by modulating the NF- $\kappa$ B-TAK1-ERK1/2 axis in the context of PPAR $\gamma$  agonistic activity. *Naunyn Schmiedebergs Arch Pharmacol*. 2019;392(12):1591–604. <https://doi.org/10.1007/s00210-019-01706-2>.
- Deppe S, Böger RH, Weiss J, Benndorf RA. Telmisartan: a review of its pharmacodynamic and pharmacokinetic properties. *Expert opinion on drug metabolism toxicology and Applied Pharmacology*. 2010;6(7):863–71. <https://doi.org/10.1517/17425255.2010.494597>.
- Avila MA, Berasain C, Sangro B, Prieto J. New therapies for hepatocellular carcinoma. *Oncogene*. 2006;25(27):3866–84. <https://doi.org/10.1038/sj.onc.1209550>.
- Chowdhury MMH, Salazar CJJ, Nurunnabi M. Recent advances in bionanomaterials for liver cancer diagnosis and treatment. *Biomaterials Science*. 2021;9(14):4821–42. <https://doi.org/10.1039/D1BM00167A>.
- Hu M, Huang L. Nanomaterial manipulation of immune microenvironment in the diseased liver. *Adv Func Mater*. 2019;29(7):1805760. <https://doi.org/10.1002/adfm.201805760>.
- Villa R, Cerroni B, Viganò L, Margheritelli S, Abolafio G, Oddo L, et al. Targeted doxorubicin delivery by chitosan-galactosylated modified polymer microbubbles to hepatocarcinoma cells. *Colloids Surf, B*. 2013;110:434–42. <https://doi.org/10.1016/j.colsurfb.2013.04.022>.
- Willoughby JL, Chan A, Sehgal A, Butler JS, Nair JK, Racie T, et al. Evaluation of GalNAc-siRNA conjugate activity in pre-clinical animal models with reduced asialoglycoprotein receptor expression. *Mol Ther*. 2018;26(1):105–14. <https://doi.org/10.1016/j.ymthe.2017.08.019>.
- Zhang P, Liu C, Wu W, Mao Y, Qin Y, Hu J, et al. Triapine/Ce6-loaded and lactose-decorated nanomicelles provide an effective chemo-photodynamic therapy for hepatocellular carcinoma through a reactive oxygen species-boosting and ferroptosis-inducing mechanism. *Chemical Engineering Journal*. 2021;425:131543. <https://doi.org/10.1016/j.cej.2021.131543>.
- Nair AB, Shah J, Al-Dhubiab BE, Patel SS, Morsy MA, Patel V, et al. Development of asialoglycoprotein receptor-targeted nanoparticles for selective delivery of gemcitabine to hepatocellular carcinoma. *Molecules*. 2019;24(24):4566. <https://doi.org/10.3390/molecules24244566>.
- Paramjot Khan NM, Kapahi H, Kumar S, Bhardwaj T, Arora S, et al. Role of polymer–drug conjugates in organ-specific delivery systems. *Journal of Drug Targeting*. 2015;23(5):387–416. <https://doi.org/10.3109/1061186X.2015.1016436>.
- Rohilla R, Garg T, Goyal AK, Rath G. Herbal and polymeric approaches for liver-targeting drug delivery: novel strategies and their significance. *Drug Delivery*. 2016;23(5):1645–61. <https://doi.org/10.3109/10717544.2014.945018>.
- Andrade F, Antunes F, Vanessa Nascimento A, Baptista da Silva S, dasNeves J, Ferreira D, et al. Chitosan formulations as carriers for therapeutic proteins. *Current drug discovery technologies*. 2011;8(3):157–72. <https://doi.org/10.2174/157016311796799035>.
- Ye B-l, Zheng R, Ruan X-j, Zheng Z-h, Cai H-j. Chitosan-coated doxorubicin nano-particles drug delivery system inhibits cell growth of liver cancer via p53/PRC1 pathway. *Biochemical and biophysical research communications*. 2018;495(1):414–20. <https://doi.org/10.1016/j.bbrc.2017.10.156>.
- Kania G, Sternak M, Jaształ A, Chlopicki S, Błażejczyk A, Nasuliewicz-Goldeman A, et al. Uptake and bioreactivity of charged chitosan-coated superparamagnetic nanoparticles as promising contrast agents for magnetic resonance imaging. *Nanomedicine: Nanotechnology Biology and Medicine*. 2018;14(1):131–40. <https://doi.org/10.1016/j.nano.2017.09.004>.
- Bonferoni MC, Gavini E, Rassu G, Maestri M, Giunchedi P. Chitosan nanoparticles for therapy and theranostics of hepatocellular carcinoma (HCC) and liver-targeting. *Nanomaterials*. 2020;10(5):870. <https://doi.org/10.3390/nano10050870>.
- Anter HM, Aman RM, Othman DIA, Elamin KM, Hashim IIA, Meshali MM. Apocynin-loaded PLGA nanomedicine tailored with galactosylated chitosan intrigue asialoglycoprotein receptor in hepatic carcinoma: Prospective targeted therapy. *International Journal of Pharmaceutics*. 2023;631:122536. <https://doi.org/10.1016/j.ijpharm.2022.122536>.
- Dhavalé RP, Dhavalé R, Sahoo S, Kollu P, Jadhav S, Patil P, et al. Chitosan coated magnetic nanoparticles as carriers of anticancer drug Telmisartan: pH-responsive controlled drug release and cytotoxicity studies. *Journal of Physics and Chemistry of Solids*. 2021;148:109749. <https://doi.org/10.1016/j.jpics.2020.109749>.
- Badano JA, Braber NV, Rossi Y, Vergara LD, Bohl L, Porporatto C, et al. Physicochemical, in vitro antioxidant and cytotoxic properties of water-soluble chitosan-lactose derivatives. *Carbohydrate polymers*. 2019;224:115158. <https://doi.org/10.1016/j.carbpol.2019.115158>.

24. Chung YC, Tsai CF, Li CF. Preparation and characterization of water-soluble chitosan produced by Maillard reaction. *Fish Sci.* 2006;72(5):1096–103. <https://doi.org/10.1111/j.1444-2906.2006.01261.x>.
25. Ying G-q, Xiong W-y, Wang H, Sun Y, Liu H-z. Preparation, water solubility and antioxidant activity of branched-chain chitosan derivatives. *Carbohydrate Polymers.* 2011;83(4):1787–96. <https://doi.org/10.1016/j.carbpol.2010.10.037>.
26. Chung Y-C, Kuo C-L, Chen C-C. Preparation and important functional properties of water-soluble chitosan produced through Maillard reaction. *Biores Technol.* 2005;96(13):1473–82. <https://doi.org/10.1016/j.biortech.2004.12.001>.
27. Czechowska-Biskup R, Jarosińska D, Rokita B, Ulański P, Rosiak JM. Determination of degree of deacetylation of chitosan-comparison of methods. *Progress on Chemistry and Application of Chitin and its Derivatives.* 2012;17:5–20.
28. Calvo P, Remuñan-López C, Vila-Jato JL, Alonso MJ. Chitosan and chitosan/ethylene oxide-propylene oxide block copolymer nanoparticles as novel carriers for proteins and vaccines. *Pharm Res.* 1997;14(10):1431–6. <https://doi.org/10.1023/A:1012128907225>.
29. Bebawy LI, Abbas SS, Fattah LA, Refaat HH. Application of first-derivative, ratio derivative spectrophotometry, TLC-densitometry and spectrofluorimetry for the simultaneous determination of telmisartan and hydrochlorothiazide in pharmaceutical dosage forms and plasma. *Il Farmaco.* 2005;60(10):859–67. <https://doi.org/10.1016/j.farmac.2005.06.009>.
30. Thapa C, Ahad A, Aqil M, Imam SS, Sultana Y. Formulation and optimization of nanostructured lipid carriers to enhance oral bioavailability of telmisartan using Box-Behnken design. *Journal of Drug Delivery Science and Technology.* 2018;44:431–9. <https://doi.org/10.1016/j.jddst.2018.02.003>.
31. Talevi A, Ruiz ME. Drug Release. In: Talevi A, editor. *The ADME Encyclopedia.* Springer; 2021. p. 1–7.
32. El-Gizawy SA, El-Maghraby GM, Hedaya AA. Formulation of acyclovir-loaded solid lipid nanoparticles: design, optimization, and in-vitro characterization. *Pharm Dev Technol.* 2019;24(10):1287–98. <https://doi.org/10.1080/10837450.2019.1667385>.
33. Nenicu A, Gu Y, Körbel C, Menger MD, Laschke MW. Combination therapy with telmisartan and parecoxib induces regression of endometriotic lesions. *Br J Pharmacol.* 2017;174(16):2623–35. <https://doi.org/10.1111/bph.13874>.
34. Mourya V, Inamdar NN. Chitosan-modifications and applications: opportunities galore. *React Funct Polym.* 2008;68(6):1013–51. <https://doi.org/10.1016/j.reactfunctpolym.2008.03.002>.
35. Fang J, Qin G, Ma J, She Y-M. Quantification of plant cell wall monosaccharides by reversed-phase liquid chromatography with 2-aminobenzamide pre-column derivatization and a non-toxic reducing reagent 2-picoline borane. *J Chromatogr A.* 2015;1414:122–8. <https://doi.org/10.1016/j.chroma.2015.08.038>.
36. Gullón B, Montenegro MI, Ruiz-Matute AI, Cardelle-Cobas A, Corzo N, Pintado ME. Synthesis, optimization and structural characterization of a chitosan–glucose derivative obtained by the Maillard reaction. *Carbohydr Polym.* 2016;137:382–9. <https://doi.org/10.1016/j.carbpol.2015.10.075>.
37. Braber NV, Vergara LD, Rossi YE, Aminahuel CA, Mauri AN, Cavaglieri LR, et al. Effect of microencapsulation in whey protein and water-soluble chitosan derivative on the viability of the probiotic *Kluyveromyces marxianus* VM004 during storage and in simulated gastrointestinal conditions. *LWT.* 2020;118:108844. <https://doi.org/10.1016/j.lwt.2019.108844>.
38. Li X, Shi X, Wang M, Du Y. Xylan chitosan conjugate—a potential food preservative. *Food Chem.* 2011;126(2):520–5. <https://doi.org/10.1016/j.foodchem.2010.11.037>.
39. Umemura K, Kawai S. Preparation and characterization of Maillard reacted chitosan films with hemicellulose model compounds. *J Appl Polym Sci.* 2008;108(4):2481–7. <https://doi.org/10.1002/app.27842>.
40. Popielarski SR, Pun SH, Davis ME. A nanoparticle-based model delivery system to guide the rational design of gene delivery to the liver 1 Synthesis and characterization. *Bioconjugate chemistry.* 2005;16(5):1063–70. <https://doi.org/10.1021/bc050113d>.
41. Rensen PC, Sliedregt LA, Ferns M, Kieviet E, Van Rossenberg SM, Van Leeuwen SH, et al. Determination of the upper size limit for uptake and processing of ligands by the asialoglycoprotein receptor on hepatocytes in vitro and in vivo. *J Biol Chem.* 2001;276(40):37577–84. <https://doi.org/10.1074/jbc.M101786200>.
42. Wu F, Wuensch SA, Azadniv M, Ebrahimkhani MR, Crispe IN. Galactosylated LDL nanoparticles: a novel targeting delivery system to deliver antigen to macrophages and enhance antigen specific T cell responses. *Mol Pharm.* 2009;6(5):1506–17. <https://doi.org/10.1021/mp900081y>.
43. El-Gizawy SA, Nouh A, Saber S, Kira AY. Deferoxamine-loaded transfersomes accelerates healing of pressure ulcers in streptozotocin-induced diabetic rats. *Journal of Drug Delivery Science and Technology.* 2020;58:101732. <https://doi.org/10.1016/j.jddst.2020.101732>.
44. Cogger VC, McNerney GP, Nyunt T, DeLeve LD, McCourt P, Smedsrød B, et al. Three-dimensional structured illumination microscopy of liver sinusoidal endothelial cell fenestrations. *J Struct Biol.* 2010;171(3):382–8. <https://doi.org/10.1016/j.jsb.2010.06.001>.
45. Li L, Wang H, Ong ZY, Xu K, Ee PLR, Zheng S, et al. Polymer and lipid-based nanoparticle therapeutics for the treatment of liver diseases. *Nano Today.* 2010;5(4):296–312. <https://doi.org/10.1016/j.nantod.2010.06.007>.
46. Liu H, Gao C. Preparation and properties of ionically cross-linked chitosan nanoparticles. *Polym Adv Technol.* 2009;20(7):613–9. <https://doi.org/10.1002/pat.1306>.
47. Wang Z, He X. Dynamics of vesicle formation from lipid droplets: mechanism and controllability. *The Journal of chemical physics.* 2009;130(9):094905. <https://doi.org/10.1063/1.3079097>.
48. Hashad RA, Ishak RA, Geneidi AS, Mansour S. Methotrexate loading in chitosan nanoparticles at a novel pH: response surface modeling, optimization and characterization. *Int J Biol Macromol.* 2016;91:630–9. <https://doi.org/10.1016/j.ijbiomac.2016.06.014>.
49. Cheng S-H, Li F-C, Souris JS, Yang C-S, Tseng F-G, Lee H-S, et al. Visualizing dynamics of sub-hepatic distribution of nanoparticles using intravital multiphoton fluorescence microscopy. *ACS Nano.* 2012;6(5):4122–31. <https://doi.org/10.1021/nn300558p>.
50. Xiao K, Li Y, Luo J, Lee JS, Xiao W, Gonik AM, et al. The effect of surface charge on in vivo biodistribution of PEG-oligocholeic acid based micellar nanoparticles. *Biomaterials.* 2011;32(13):3435–46. <https://doi.org/10.1016/j.biomaterials.2011.01.021>.
51. Poelstra K, Prakash J, Beljaars L. Drug targeting to the diseased liver. *J Control Release.* 2012;161(2):188–97. <https://doi.org/10.1016/j.jconrel.2012.02.011>.
52. Delan WK, Zakaria M, Elsaadany B, ElMeshad AN, Mamdouh W, Fares AR. Formulation of simvastatin chitosan nanoparticles for controlled delivery in bone regeneration: Optimization using Box-Behnken design, stability and in vivo study. *International journal of pharmaceuticals.* 2020;577:119038. <https://doi.org/10.1016/j.ijpharm.2020.119038>.

53. Sreeharsha N, Rajpoot K, Tekade M, Kalyane D, Nair AB, Venugopala KN, et al. Development of metronidazole loaded chitosan nanoparticles using QbD approach—a novel and potential antibacterial formulation. *Pharmaceutics*. 2020;12(10):920. <https://doi.org/10.3390/pharmaceutics12100920>.
54. Wu Y, Yang W, Wang C, Hu J, Fu S. Chitosan nanoparticles as a novel delivery system for ammonium glycyrrhizinate. *Int J Pharm*. 2005;295(1–2):235–45. <https://doi.org/10.1016/j.ijpharm.2005.01.042>.
55. Verma A, Stellacci F. Effect of surface properties on nanoparticle–cell interactions. *small*. 2010;6(1):12–21. <https://doi.org/10.1002/sml.200901158>.
56. Kaasalainen M, Aseyev V, von Haartman E, Karaman DŞ, Mäkilä E, Tenhu H, et al. Size, stability, and porosity of mesoporous nanoparticles characterized with light scattering. *Nanoscale Res Lett*. 2017;12(1):1–10. <https://doi.org/10.1186/s11671-017-1853-y>.
57. Ganesh M, Ubaidulla U, Rathnam G, Jang HT. Chitosan-telmisartan polymeric cocrystals for improving oral absorption: in vitro and in vivo evaluation. *Int J Biol Macromol*. 2019;131:879–85. <https://doi.org/10.1016/j.ijbiomac.2019.03.141>.
58. Mhetre RL, Hol VB, Chanshetty R, Dhole SN. Tailoring of anti-hypertensive drug-loaded nanoparticles: in vitro, toxicity, and bioavailability assessment. *BioNanoScience*. 2022;12(1):28–40. <https://doi.org/10.1007/s12668-021-00910-w>.
59. Khanfar M, Al-Remawi M, Al-Akayleh F, Hmouze S. Preparation and evaluation of co-amorphous formulations of telmisartan—amino acids as a potential method for solubility and dissolution enhancement. *AAPS PharmSciTech*. 2021;22(3):1–13. <https://doi.org/10.1208/s12249-021-01952-9>.
60. Ulbrich K, Hola K, Subr V, Bakandritsos A, Tucek J, Zboril R. Targeted drug delivery with polymers and magnetic nanoparticles: covalent and noncovalent approaches, release control, and clinical studies. *Chem Rev*. 2016;116(9):5338–431. <https://doi.org/10.1021/acs.chemrev.5b00589>.
61. Yin H, Lee ES, Kim D, Lee KH, Oh KT, Bae YH. Physicochemical characteristics of pH-sensitive poly (L-histidine)-b-poly (ethylene glycol)/poly (L-lactide)-b-poly (ethylene glycol) mixed micelles. *J Control Release*. 2008;126(2):130–8. <https://doi.org/10.1016/j.jconrel.2007.11.014>.
62. Tsai ML, Bai SW, Chen RH. Cavitation effects versus stretch effects resulted in different size and polydispersity of ionotropic gelation chitosan–sodium tripolyphosphate nanoparticle. *Carbohydr Polym*. 2008;71(3):448–57. <https://doi.org/10.1016/j.carbpol.2007.06.015>.
63. Szymańska E, Winnicka K. Stability of chitosan—a challenge for pharmaceutical and biomedical applications. *Mar Drugs*. 2015;13(4):1819–46. <https://doi.org/10.3390/md13041819>.
64. Shimizu K, Takashima T, Yamane T, Sasaki M, Kageyama H, Hashizume Y, et al. Whole-body distribution and radiation dosimetry of [<sup>11</sup>C] telmisartan as a biomarker for hepatic organic anion transporting polypeptide (OATP) 1B3. *Nucl Med Biol*. 2012;39(6):847–53. <https://doi.org/10.1016/j.nucmedbio.2012.01.008>.

**Publisher's Note** Springer Nature remains neutral with regard to jurisdictional claims in published maps and institutional affiliations.